

Thermodynamic Modeling Study of Carbonation of Portland Cement

Kamasani Chiranjeevi Reddy , Nahom S. Melaku  and Solmoi Park * 

Department of Civil Engineering, Pukyong National University, 45 Yongso-ro, Nam-gu, Busan 48513, Korea; kc.reddy@pknu.ac.kr (K.C.R.); naspknu@pukyong.ac.kr (N.S.M.)

* Correspondence: solmoi.park@pknu.ac.kr; Tel.: +82-51-629-6066

Abstract: The assessment of the extent of carbonation and related phase changes is important for the evaluation of the durability aspects of concrete. The phase assemblage of Portland cements with different clinker compositions is evaluated using thermodynamic calculations. Four different compositions of cements, as specified by ASTM cements types I to IV, are considered in this study. Calcite, zeolites, and gypsum were identified as carbonation products. CO₂ content required for full carbonation had a direct relationship with the initial volume of phases. The CO₂ required for portlandite determined the initiation of carbonation of C-S-H. A continual decrease in the pH of pore solution and a decrease in Ca/Si is observed with the carbonation of C-S-H. Type II cement exhibited rapid carbonation at relatively less CO₂ for full carbonation, while type III required more CO₂ to carbonate to the same level as other types of cement. The modeling of carbonation of different Portland cements provided insights into the quantity of CO₂ required to destabilize different hydrated products into respective carbonated phases.

Keywords: Portland cement; carbonation; thermodynamic modeling; phase evolution



Citation: Reddy, K.C.; Melaku, N.S.; Park, S. Thermodynamic Modeling Study of Carbonation of Portland Cement. *Materials* **2022**, *15*, 5060. <https://doi.org/10.3390/ma15145060>

Academic Editors: Milica Vasic and Anja Terzic

Received: 24 June 2022

Accepted: 15 July 2022

Published: 20 July 2022

Publisher's Note: MDPI stays neutral with regard to jurisdictional claims in published maps and institutional affiliations.



Copyright: © 2022 by the authors. Licensee MDPI, Basel, Switzerland. This article is an open access article distributed under the terms and conditions of the Creative Commons Attribution (CC BY) license (<https://creativecommons.org/licenses/by/4.0/>).

1. Introduction

The interaction of CO₂ with hydrated cement induces various physiochemical changes in the hydration products and unreacted clinker. Carbon dioxide present in the ambient environment diffuses through the capillary pores of cement and is dissolved in pore solution, resulting in the carbonates at pH ≥ 9 and bicarbonates at 6 ≤ pH ≤ 8 [1,2]. The carbonate ions primarily interact with calcium in hydration products, resulting in the precipitation of calcium carbonate [3]. The formation of carbonates, bicarbonates, and the consumption of calcium during the carbonation reaction results in a decrease in pH [4–6]. At these reduced pH levels, the protective oxide layer becomes unstable and exposes reinforcing steel to corrosion [7,8]. Hence, carbonation is one of the most important durability properties to accurately evaluate.

The carbonation of concrete can happen at a wide variety of exposures. Natural carbonation that occurs at atmospheric pressure (PCO₂—3.55 × 10^{−4} bars) is a very slow process and can progress for many years. Carbonation at higher partial pressures of CO₂ can accelerate the carbonation rate and help our understanding of the phase change phenomenon over a short period [9]. However, accelerated carbonation can be carried out at various CO₂ increments by the mass of the binder, and is related to natural carbonation [3]. Alternatively, mathematical models, kinetic models, and thermodynamic models can be employed to quickly predict the phase assemblage resulting from the carbonation of Portland cement [10–12].

Thermodynamic calculations and modelling were shown to reliably predict the hydrate assemblage upon complete hydration, changes in solid phase composition and pore solution composition in cementitious systems [13,14]. Numerous studies have employed thermodynamic modelling in assessing phase changes in Portland cement systems with

mineral additions such as limestone, clay, fly ash, and slag [15–21]. Thermodynamic simulations were also applied to predict the hydrate assemblage in alternate cements such as calcium sulfoaluminate cements [22–26] and alkali-activated slag systems [27–29]. In addition, thermodynamic calculations are very convenient for assessing the durability performance of cementitious systems. They have been extensively used in predicting phase changes as a function of chloride content using NaCl and sea water in PC systems [30,31] and as a function of CO₂ in hydrated PC and PC blends subjected to carbonation [32,33].

The extent of the carbonation of cement mainly depends on the diffusion capacity of CO₂, which in turn depends on the porosity and pore size distribution [4,9]. The carbonation of plain PC primarily happens in portlandite, resulting in CaCO₃ precipitation and a subsequent decrease in pore size, thereby negating accelerated carbonation in PC [33–35]. Portlandite buffers the pore solution pH by supplying [OH⁻] ions and the amount of portlandite determines the onset of carbonation of C-S-H [32,36]. The stability of different phases of hydrated cement depends on the pore solution pH and is destabilized at various pH concentrations when the pH drops below the corresponding threshold value [37]. Thus, the relative proportions of hydrated phases present in hydrated cement tend to influence the onset and extent of carbonation. Hence, it is essential to study the carbonation behavior of hydrated cement with different clinker compositions.

In this study, the carbonation behavior and related changes in phase assemblage of ASTM cement types I-IV were studied using thermodynamic modeling. ASTM types of cement differ in clinker composition, and thus result in hydration products with different proportions, thereby altering the extent of carbonation.

2. Materials and Methods

Four types of Portland cement were used in the simulation of the carbonation of Portland cement with a water to cement ratio of 0.8. Up to 40% CO₂ was added by the mass of cement. A high water-to-cement ratio was used, as it was the minimum ratio that satisfied the mass balance requirement of the whole mixture for the given CO₂ quantity. The composition of each type of cement is indicated in Table 1. The reaction degree of the clinkers after 28 days of hydration was predicted using Parrot and Killoh’s hydration model and used in the carbonation simulation.

Table 1. Composition of PC (expressed in mass %).

	C ₃ S	C ₂ S	C ₃ A	C ₄ AF	CaSO ₄	Other Phases
Type I	55	19	10	7	4.2	4.8
Type II	51	24	6	11	3.3	4.7
Type III	57	17.7	10	7	3.1	5.2
Type IV	38	43	4	9	2.4	3.6

Thermodynamic calculations were made using GEM-Selektor v.3.7 [38,39] and CEM-DATA18 [40]. The activity coefficients were calculated using the following equation [41]:

$$\log_{10}\gamma_i = \frac{-A_\gamma z_i^2 \sqrt{I}}{1 + aB_\gamma \sqrt{I}} + b_\gamma I + \log_{10} \frac{X_{jw}}{X_w} \quad (1)$$

where γ_i and z_i represent the activity coefficient and charge of the i^{th} species, respectively. A_γ and B_γ are coefficients dependent on temperature and pressure, respectively. The effective molal ionic strength is given by I . X_{jw} and X_w are the molar quantity of water and total aqueous phase, respectively. Common ion size parameter (a) and short-range interaction parameter (b_γ), were set to 3.67 Å and 1.23 kg/mol, respectively, using KOH as the background electrolyte.

3. Results

The predicted phase assemblages of Portland cement during carbonation are shown in Figure 1 as a function of carbonation extent. C-S-H and portlandite are the major hydration products that are present along with unreacted clinker. Fe-hydrogarnet, monosulphate, and ettringite were the minor phases. The modeling results for the carbonation of all types of Portland cement predict the formation of calcite, zeolites, and gypsum as carbonation products [42,43]. While calcite started forming at a lower carbonation extent, the gypsum and zeolites precipitated at a higher carbonation extent. Strätlingite formed as a transient phase at a higher carbonation extent. The extent of carbonation was observed to depend on the type of cement.

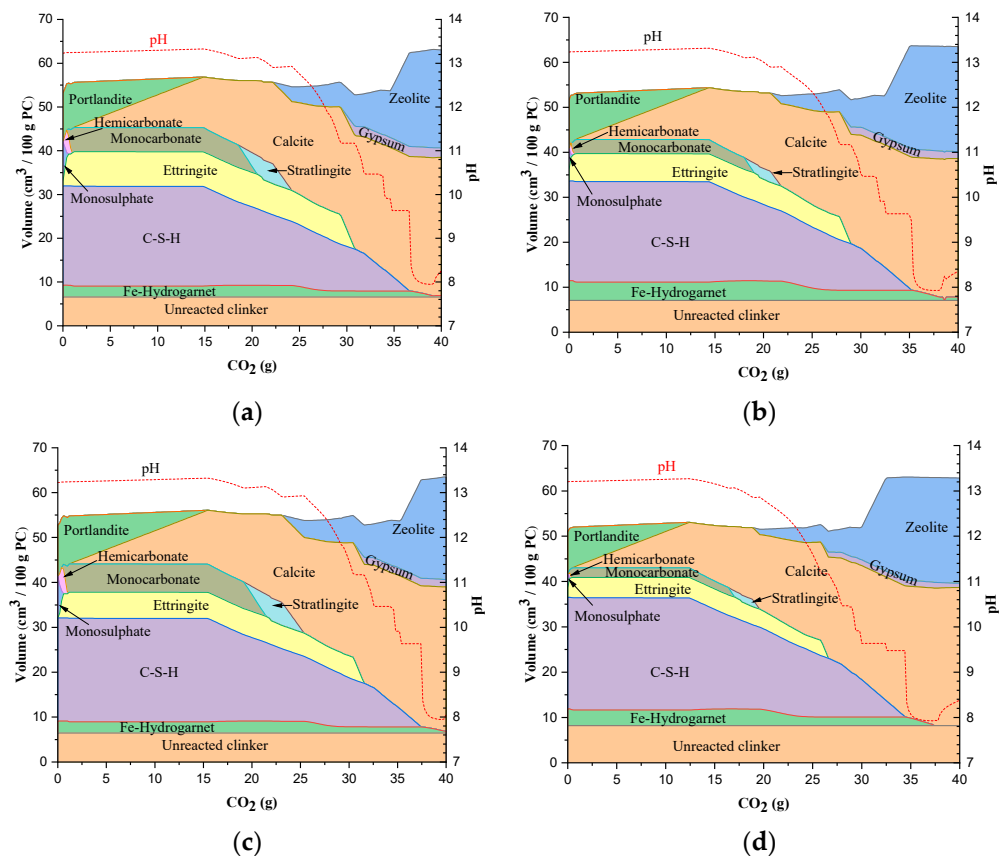
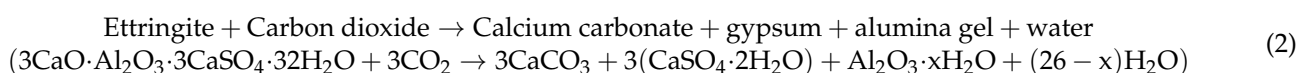


Figure 1. Simulation of carbonation of Portland cement: (a) type I, (b) type II, (c) type III and (d) type IV.

The phase volume change in type I cement as a function of carbonation extent is shown in Figure 1a. Portlandite and monosulphate started to destabilize upon exposure to very little CO_2 , resulting in the formation of hemicarbonate and ettringite. Hemicarbonate further destabilized into monocarbonate, a more stable phase upon the complete destabilization of monosulphate, with an increase in the carbonation extent. The destabilization of portlandite continued until its depletion at an increased carbonation extent. Calcite is the prominent carbonate phase resulting from the destabilization of portlandite; however, the calcite precipitation is initiated upon the complete destabilization of hemicarbonate to monocarbonate. The volume of ettringite increased during monosulphate destabilization and remained constant up to carbonation extent of ~ 30 g per 100 g cement and then destabilized into gypsum. The kinetics of ettringite destabilization can be expressed with the following equation [44,45]:



The destabilization of C-S-H is triggered with the complete depletion of portlandite and continues until its completion. Calcite is the carbonate phase resulting from the C-S-H destabilization. The pH of the pore solution also started to decline during the carbonation of C-S-H [46]. With a small decrease in pH from 13.3 to 13.1, the monocarbonate is destabilized into strätlingite. Strätlingite is a gehlenite hydrate with a typical composition as $\text{Ca}_2\text{Al}_2\text{SiO}_7 \cdot 8\text{H}_2\text{O}$ and is precipitated from the alumina and silica released by the monocarbonate and C-S-H decomposition, respectively. While the pH is constant during strätlingite formation, it further decreased and reached a small plateau during the destabilization of strätlingite and simultaneous precipitation of zeolites at a pH of ~ 12.9 . Thereafter, the pH rapidly decreased to a value of ~ 11.2 and again reached a plateau where the ettringite destabilization was initiated. The destabilization of ettringite resulted in the formation of gypsum along with calcite. The volume of zeolites increased close to the complete destabilization of C-S-H. The pH is constant during the precipitation of zeolites; however, it decreased drastically upon the complete consumption of C-S-H. The formation of zeolites is mainly attributed to the destabilization of strätlingite and C-S-H coupled with the availability of alkali metals in the pore solution. The formation of zeolites reduces the alkali metal ions in the pore solution, resulting in the decrease in pH [32]. Fe-hydrogarnet partially destabilized into calcite after strätlingite consumption, while its complete destabilization occurred after the total carbonation of C-S-H.

The volume changes in different phases in hydrated type II cement when exposed to CO_2 are shown in Figure 1b. Type II cement has a lower amount of hydration products with the exception of Fe-hydrogarnet and ettringite compared to type I cement. Portlandite and monosulphate begin to carbonate immediately, as noticed in the previous case. Monosulphate is completely destabilized to ettringite and hemicarbonate. At a similar extent of carbonation with that of type I cement, monocarbonate started to precipitate. A small decrease in the hydrogarnet volume is observed during decomposition of hemicarbonate.

While the relative trends in carbonation of different phases are similar to the type I cement, the initial volume of phases determined the amount of CO_2 required for the full carbonation. The complete carbonation of portlandite in type II occurred at a relatively lower extent of carbonation when compared to type I (i.e., 14.6 g CO_2). This initiated the early destabilization of C-S-H and a decrease in the pH value in the system from 13.3. The destabilization of monocarbonate to strätlingite, and further destabilization of strätlingite to calcite and zeolites were also advanced. Ettringite destabilization is also initiated at a lower carbonation extent. The complete carbonation of C-S-H to calcite in type II cement is also advanced, thus causing the destabilization of Fe-hydrogarnet. The changes in pH in type II cement followed a similar pattern to that of type I cement; however, the decrease in pH occurred at a lower carbonation extent compared to type I cement, owing to the lower quantity of hydration products.

Figure 1c shows the changes in the volume of different phases in type III cement in the CO_2 environment. Type III cement has the highest amount of hydration products compared to the other cement types. As a result, the CO_2 content required to destabilize the phases into their respective stable phases was higher compared to the other types of cement. Ettringite, unlike in other types of cements, was not a hydration product but precipitated through destabilization of monosulphate to monocarbonate via hemicarbonate. The destabilization of phases at various levels of CO_2 and changes in the pore solution pH follow a similar trend to that of type I and type II cements. The last type of cement, type IV, has the lowest amount of hydration products with the exception of C-S-H. It has a highest amount of C-S-H which can be attributed to the higher amount of C_2S . The volume changes in phases of type IV cement during carbonation are shown in Figure 1d. The lesser volume of hydration phases resulted in the carbonation of phases at lower contents of CO_2 than the other types of cement.

The change in the Ca/Si ratio of C-S-H during the simulated carbonation is shown in Figure 2. The volume of C-S-H is constant during the carbonation of portlandite, as the portlandite preferentially undergoes carbonation and acts as a buffer for C-S-H [47].

Therefore, the Ca/Si ratio of C-S-H is constant as long as portlandite is present in the system. Upon the consumption of portlandite, C-S-H starts destabilizing into calcite resulting in Si-rich C-S-H gel with a continuous decrease in the Ca/Si ratio, until the destabilization of monocarbonate is initiated. During the destabilization of monocarbonate to strätlingite, the Ca/Si ratio is constant. The precipitation of strätlingite consumes the Si released by the carbonation of C-S-H, thereby offsetting the decrease in the Ca/Si ratio of C-S-H. The Ca/Si ratio of C-S-H continues to decrease upon the complete stabilization of strätlingite until the destabilization of strätlingite is initiated. The Si released from the combined carbonation of C-S-H and destabilization of strätlingite along with Al from strätlingite is used in the stabilization of zeolites, and this ensures a constant Ca/Si during the destabilization of strätlingite. The Ca/Si ratio continues to decrease after the complete carbonation of strätlingite till the conversion of ettringite into gypsum is initiated. During the destabilization of ettringite, the Al released from ettringite and Si from C-S-H again results in zeolites, leading to a constant Ca/Si ratio of C-S-H. The Ca/Si further decreases post ettringite carbonation and reaches a plateau when C-S-H quantity becomes very low. The increase in the volume of zeolites is observed during the constant Ca/Si ratio of C-S-H prior to the complete carbonation of C-S-H.

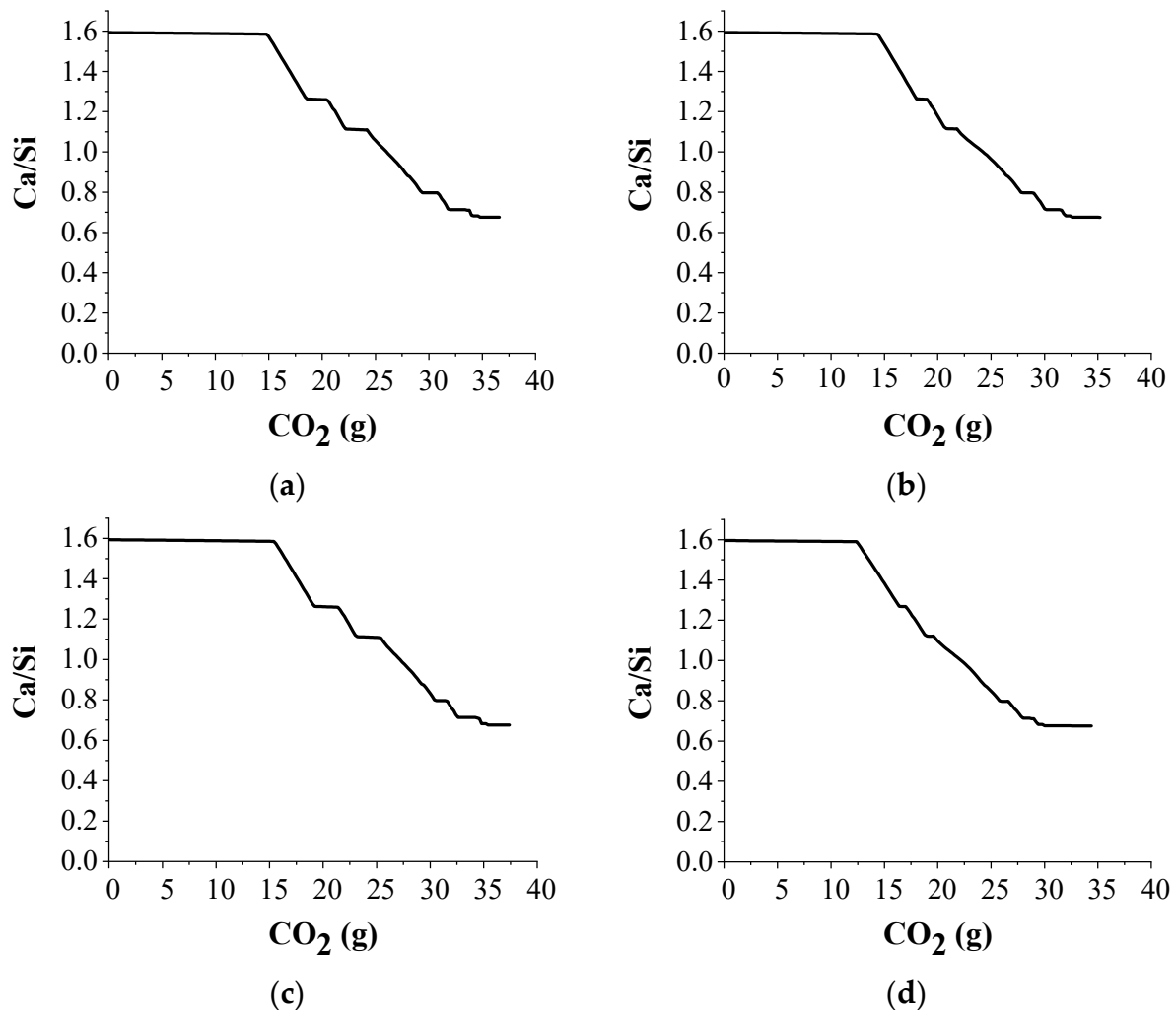


Figure 2. Change in the Ca/Si ratio of C-S-H during carbonation. (a) type I, (b) type II, (c) type III, (d) type IV.

4. Conclusions

This study investigated the effect of the chemical compositions of cements on the phase evolution during carbonation using thermodynamic calculations. The outcomes of this study can be summarized as follows.

- (1) Calcite is the major carbonation product. Zeolites and gypsum were observed as other minor carbonation phases, while the carbonation of the major hydration products resulted in calcite and the destabilization of strätlingite and C-S-H, along with the alkali metal ions present in the pore solution, resulted in zeolites. On the other hand, the formation of gypsum is solely linked to the destabilization of ettringite.
- (2) The initial volume of each phase determined the CO₂ content required for their full carbonation. The higher the initial volume, the larger the CO₂ content required for full carbonation.
- (3) The extent of CO₂ required for the initiation of C-S-H carbonation has a direct relationship with portlandite quantity. Pore solution pH and Ca/Si of C-S-H continually decreased with the carbonation of C-S-H.
- (4) The carbonation of type II cement is rapid and progressed at a relatively lower CO₂ content, while type III had a higher demand of CO₂ for a similar extent of carbonation compared to other types of cements. The volume of hydration products prior to carbonation determined the quantity of CO₂ required for complete carbonation.
- (5) Type IV cement required a greater content of CO₂ for complete carbonation of C-S-H owing to the highest content of C-S-H.

The results reveal that a higher portlandite content delays the carbonation of C-S-H and the quantity of C-S-H itself determines the amount of CO₂ required for its complete destabilization. The clinker composition, which can result in large quantities of portlandite and C-S-H can be most effective under carbonation conditions. With further studies, the type of cement with the best mechanical CO₂ resistance and other durability performances can be recommended. Further experimental programs can be designed to include compressive strength tests, XRD and TGA profiling, and other microstructure evaluation techniques on carbonated PC and its blends with other cementitious materials for a de-tailed understanding of the carbonation mechanism and its effect on strength and durability.

Author Contributions: Conceptualization, K.C.R., N.S.M. and S.P.; Data curation, N.S.M. and S.P.; Formal analysis, K.C.R., N.S.M.; Funding acquisition, S.P.; Investigation, N.S.M.; Methodology, K.C.R.; Project administration, S.P.; Supervision, S.P.; Writing—original draft, K.C.R.; Writing—review & editing, N.S.M. and S.P. All authors have read and agreed to the published version of the manuscript.

Funding: This study was supported by Korea Institute of Energy Technology Evaluation and Planning (KETEP) grant funded by the Korea Government (MOTIE) (No. 20212010200080, In situ carbonation technology development using CO₂ emissions from cement industry), and by a grant (21CTAP-C163988-01) from Ministry of Land, Infrastructure and Transport (MOLIT) of Korea Government and Korea Agency for Infrastructure Technology Advancement (KAIA).

Data Availability Statement: The data are available upon request.

Conflicts of Interest: The authors declare no conflict of interest.

References

1. Kern, D.M. The Hydration of Carbon Dioxide. *J. Chem. Educ.* **1960**, *37*, 14. [[CrossRef](#)]
2. Zeebe, R.E.; Wolf-Gladrow, D. *CO₂ in Seawater: Equilibrium, Kinetics, Isotopes*; Gulf Professional Publishing: Houston, TX, USA, 2001; ISBN 0444509461.
3. Castellote, M.; Fernandez, L.; Andrade, C.; Alonso, C. Chemical Changes and Phase Analysis of OPC Pastes Carbonated at Different CO₂ Concentrations. *Mater. Struct.* **2009**, *42*, 515–525. [[CrossRef](#)]
4. Von Greve-Dierfeld, S.; Lothenbach, B.; Vollpracht, A.; Wu, B.; Huet, B.; Andrade, C.; Medina, C.; Thiel, C.; Gruyaert, E.; Vanoutrive, H.; et al. Understanding the Carbonation of Concrete with Supplementary Cementitious Materials: A Critical Review by RILEM TC 281-CCC. *Mater. Struct.* **2020**, *53*, 136. [[CrossRef](#)]
5. Moon, E.-J.; Choi, Y.C. Carbon Dioxide Fixation via Accelerated Carbonation of Cement-Based Materials: Potential for Construction Materials Applications. *Constr. Build. Mater.* **2019**, *199*, 676–687. [[CrossRef](#)]

6. Anstice, D.J.; Page, C.L.; Page, M.M. The Pore Solution Phase of Carbonated Cement Pastes. *Cem. Concr. Res.* **2005**, *35*, 377–383. [[CrossRef](#)]
7. Glass, G.K.; Page, C.L.; Short, N.R. Factors Affecting the Corrosion Rate of Steel in Carbonated Mortars. *Corros. Sci.* **1991**, *32*, 1283–1294. [[CrossRef](#)]
8. Belda Revert, A.; De Weerd, K.; Hornbostel, K.; Geiker, M.R. Carbonation-Induced Corrosion: Investigation of the Corrosion Onset. *Constr. Build. Mater.* **2018**, *162*, 847–856. [[CrossRef](#)]
9. Wang, J.; Xu, H.; Xu, D.; Du, P.; Zhou, Z.; Yuan, L.; Cheng, X. Accelerated Carbonation of Hardened Cement Pastes: Influence of Porosity. *Constr. Build. Mater.* **2019**, *225*, 159–169. [[CrossRef](#)]
10. You, X.; Hu, X.; He, P.; Liu, J.; Shi, C. A Review on the Modelling of Carbonation of Hardened and Fresh Cement-Based Materials. *Cem. Concr. Compos.* **2022**, *125*, 104315. [[CrossRef](#)]
11. Chen, D.; Liu, S.; Shen, J.; Sun, G.; Shi, J. Experimental Study and Modelling of Concrete Carbonation under the Coupling Effect of Freeze-Thaw Cycles and Sustained Loads. *J. Build. Eng.* **2022**, *52*, 104390. [[CrossRef](#)]
12. Guo, B.; Qiao, G.; Han, P.; Li, Z.; Fu, Q. Effect of Natural Carbonation on Chloride Binding Behaviours in OPC Paste Investigated by a Thermodynamic Model. *J. Build. Eng.* **2022**, *49*, 104021. [[CrossRef](#)]
13. Lothenbach, B.; Zajac, M. Application of Thermodynamic Modelling to Hydrated Cements. *Cem. Concr. Res.* **2019**, *123*, 105779. [[CrossRef](#)]
14. Damidot, D.; Lothenbach, B.; Herfort, D.; Glasser, F.P. Thermodynamics and Cement Science. *Cem. Concr. Res.* **2011**, *41*, 679–695. [[CrossRef](#)]
15. De Weerd, K.; Haha, M.B.; Le Saout, G.; Kjellsen, K.O.; Justnes, H.; Lothenbach, B. Hydration Mechanisms of Ternary Portland Cements Containing Limestone Powder and Fly Ash. *Cem. Concr. Res.* **2011**, *41*, 279–291. [[CrossRef](#)]
16. Antoni, M.; Rossen, J.; Martirena, F.; Scrivener, K. Cement Substitution by a Combination of Metakaolin and Limestone. *Cem. Concr. Res.* **2012**, *42*, 1579–1589. [[CrossRef](#)]
17. Durdziński, P.T.; Ben Haha, M.; Zajac, M.; Scrivener, K.L. Phase Assemblage of Composite Cements. *Cem. Concr. Res.* **2017**, *99*, 172–182. [[CrossRef](#)]
18. Elakneswaran, Y.; Owaki, E.; Miyahara, S.; Ogino, M.; Maruya, T.; Nawa, T. Hydration Study of Slag-Blended Cement Based on Thermodynamic Considerations. *Constr. Build. Mater.* **2016**, *124*, 615–625. [[CrossRef](#)]
19. Fernández, Á.; Lothenbach, B.; Alonso, M.C.; García Calvo, J.L. Thermodynamic Modelling of Short and Long Term Hydration of Ternary Binders. Influence of Portland Cement Composition and Blast Furnace Slag Content. *Constr. Build. Mater.* **2018**, *166*, 510–521. [[CrossRef](#)]
20. Park, K.-B.; Wang, Y.-S.; Wang, X.-Y. Property Analysis of Slag Composite Concrete Using a Kinetic–Thermodynamic Hydration Model. *Appl. Sci.* **2021**, *11*, 7191. [[CrossRef](#)]
21. Yoon, H.N.; Seo, J.; Kim, S.; Lee, H.K.; Park, S. Characterization of Blast Furnace Slag-Blended Portland Cement for Immobilization of Co. *Cem. Concr. Res.* **2020**, *134*, 106089. [[CrossRef](#)]
22. Winnefeld, F.; Lothenbach, B. Hydration of Calcium Sulfoaluminate Cements—Experimental Findings and Thermodynamic Modelling. *Cem. Concr. Res.* **2010**, *40*, 1239–1247. [[CrossRef](#)]
23. Jeong, Y.; Hargis, C.; Chun, S.; Moon, J. Effect of Calcium Carbonate Fineness on Calcium Sulfoaluminate-Belite Cement. *Materials* **2017**, *10*, 900. [[CrossRef](#)] [[PubMed](#)]
24. Jeong, Y.; Hargis, C.W.; Kang, H.; Chun, S.-C.; Moon, J. The Effect of Elevated Curing Temperatures on High Ye’elite Calcium Sulfoaluminate Cement Mortars. *Materials* **2019**, *12*, 1072. [[CrossRef](#)]
25. Park, S.; Lee, N.; An, G.-H.; Koh, K.-T.; Ryu, G.-S. Modeling the Effect of Alternative Cementitious Binders in Ultra-High-Performance Concrete. *Materials* **2021**, *14*, 7333. [[CrossRef](#)]
26. Park, S.; Jeong, Y.; Moon, J.; Lee, N. Hydration Characteristics of Calcium Sulfoaluminate (CSA) Cement/Portland Cement Blended Pastes. *J. Build. Eng.* **2021**, *34*, 101880. [[CrossRef](#)]
27. Myers, R.J.; Lothenbach, B.; Bernal, S.A.; Provis, J.L. Thermodynamic Modelling of Alkali-Activated Slag Cements. *Appl. Geochem.* **2015**, *61*, 233–247. [[CrossRef](#)]
28. Criado, M.; Walkley, B.; Ke, X.; Provis, J.; Bernal, S. Slag and Activator Chemistry Control the Reaction Kinetics of Sodium Metasilicate-Activated Slag Cements. *Sustainability* **2018**, *10*, 4709. [[CrossRef](#)]
29. Park, S.; Park, H.M.; Yoon, H.N.; Seo, J.; Yang, C.M.; Provis, J.L.; Yang, B. Hydration Kinetics and Products of MgO-Activated Blast Furnace Slag. *Constr. Build. Mater.* **2020**, *249*, 118700. [[CrossRef](#)]
30. De Weerd, K.; Lothenbach, B.; Geiker, M.R. Comparing Chloride Ingress from Seawater and NaCl Solution in Portland Cement Mortar. *Cem. Concr. Res.* **2019**, *115*, 80–89. [[CrossRef](#)]
31. Jensen, M.M.; De Weerd, K.; Johannesson, B.; Geiker, M.R. Use of a Multi-Species Reactive Transport Model to Simulate Chloride Ingress in Mortar Exposed to NaCl Solution or Sea-Water. *Comput. Mater. Sci.* **2015**, *105*, 75–82. [[CrossRef](#)]
32. De Weerd, K.; Plusquellec, G.; Belda Revert, A.; Geiker, M.R.; Lothenbach, B. Effect of Carbonation on the Pore Solution of Mortar. *Cem. Concr. Res.* **2019**, *118*, 38–56. [[CrossRef](#)]
33. Shah, V.; Scrivener, K.; Bhattacharjee, B.; Bishnoi, S. Changes in Microstructure Characteristics of Cement Paste on Carbonation. *Cem. Concr. Res.* **2018**, *109*, 184–197. [[CrossRef](#)]
34. Shah, V.; Bishnoi, S. Carbonation Resistance of Cements Containing Supplementary Cementitious Materials and Its Relation to Various Parameters of Concrete. *Constr. Build. Mater.* **2018**, *178*, 219–232. [[CrossRef](#)]
35. Morandeau, A.; Thiéry, M.; Dangla, P. Investigation of the Carbonation Mechanism of CH and C-S-H in Terms of Kinetics, Microstructure Changes and Moisture Properties. *Cem. Concr. Res.* **2014**, *56*, 153–170. [[CrossRef](#)]

36. Visser, J.H.M. Influence of the Carbon Dioxide Concentration on the Resistance to Carbonation of Concrete. *Constr. Build. Mater.* **2014**, *67*, 8–13. [[CrossRef](#)]
37. Lagerblad, B. *Carbon Dioxide Uptake during Concrete Life Cycle: State of the Art*; Swedish Cement and Concrete Research Institute Stockholm: Stockholm, Sweden, 2005; ISBN 9197607002.
38. Kulik, D.A.; Wagner, T.; Dmytrieva, S.V.; Kosakowski, G.; Hingerl, F.F.; Chudnenko, K.V.; Berner, U.R. GEM-Selektor Geochemical Modeling Package: Revised Algorithm and GEMS3K Numerical Kernel for Coupled Simulation Codes. *Comput. Geosci.* **2012**, *17*, 1–24. [[CrossRef](#)]
39. Wagner, T.; Kulik, D.A.; Hingerl, F.F.; Dmytrieva, S.V. Gem-selektor geochemical modeling package: Tsolmod library and data interface for multicomponent phase models. *Can. Mineral.* **2012**, *50*, 1173–1195. [[CrossRef](#)]
40. Lothenbach, B.; Kulik, D.A.; Matschei, T.; Balonis, M.; Baquerizo, L.; Dilnesa, B.; Miron, G.D.; Myers, R.J. Cemdata18: A Chemical Thermodynamic Database for Hydrated Portland Cements and Alkali-Activated Materials. *Cem. Concr. Res.* **2019**, *115*, 472–506. [[CrossRef](#)]
41. Helgeson, H.C.; Kirkham, D.H.; Flowers, G.C. Theoretical Prediction of the Thermodynamic Behavior of Aqueous Electrolytes by High Pressures and Temperatures; IV, Calculation of Activity Coefficients, Osmotic Coefficients, and Apparent Molal and Standard and Relative Partial Molal Properties to 600 D. *Am. J. Sci.* **1981**, *281*, 1249–1516. [[CrossRef](#)]
42. Zajac, M.; Skibsted, J.; Skocek, J.; Durdzinski, P.; Bullerjahn, F.; Haha, M.B. Phase Assemblage and Microstructure of Cement Paste Subjected to Enforced, Wet Carbonation. *Cem. Concr. Res.* **2020**, *130*, 105990. [[CrossRef](#)]
43. Glasser, F.P.; Matschei, T. Interactions between Portland Cement and Carbon Dioxide. In Proceedings of the 12th ICCI Conference, Montreal, QC, Canada, 8–13 July 2007.
44. Lam, N.N. Microstructure of Ettringite Binder Exposed to Natural Carbonation. *IOP Conf. Ser. Earth Environ. Sci.* **2020**, *505*, 012002. [[CrossRef](#)]
45. Nishikawa, T.; Suzuki, K.; Ito, S.; Sato, K.; Takebe, T. Decomposition of Synthesized Ettringite by Carbonation. *Cem. Concr. Res.* **1992**, *22*, 6–14. [[CrossRef](#)]
46. Shi, Z.; Lothenbach, B.; Geiker, M.R.; Kaufmann, J.; Leemann, A.; Ferreira, S.; Skibsted, J. Experimental Studies and Thermodynamic Modeling of the Carbonation of Portland Cement, Metakaolin and Limestone Mortars. *Cem. Concr. Res.* **2016**, *88*, 60–72. [[CrossRef](#)]
47. Palacios, M.; Puertas, F. Effect of Carbonation on Alkali-Activated Slag Paste. *J. Am. Ceram. Soc.* **2006**, *89*, 3211–3221. [[CrossRef](#)]